ELSEVIER

Journal of Molecular Liquids 117 (2005) 33–41

journal of MOLECULAR LIQUIDS

www.elsevier.com/locate/molliq

Investigation of the vapor–liquid equilibrium and supercritical phase of pure methane via computer simulations

Ioannis Skarmoutsos, Leonidas I. Kampanakis, Jannis Samios*

University of Athens, Department of Chemistry, Laboratory of Physical Chemistry, Panepistimiopolis 157-71, Athens, Greece

Available online 18 October 2004

Abstract

The Gibbs Ensemble Monte Carlo (GEMC) simulation technique was used to study the vapor–liquid equilibrium (VLE) of pure methane in a wide range of thermodynamic state points. The properties of the pure fluid were also studied at supercritical (SC) conditions by performing NVT and NPT molecular dynamics (MD) simulations. Previously developed intermolecular potential models were employed to model the fluid and their properties were obtained and compared with available experimental data. The simulations have shown that a simple one site Lennard–Jones (LJ) potential model [B. Saager and J. Fischer, Fluid Phase Equil. 57 (1990) 35, J. Fischer, R. Lustig, H. Breitenfelder_Manske and W. Lemming, Mol. Phys. 52 (1984) 485.] provides accurate descriptions of the VLE state points. It is also suggested that for the accurate description of the fluid properties at SC conditions, one needs to employ all-atom (AA) interaction potentials to model the system. The effectiveness of such kind of potential models used in this study has been presented and discussed.

Keywords: Methane; Supercritical; Gibbs Ensemble Monte Carlo; Molecular dynamics

1. Introduction

During the last two decades, the properties of fluid methane have been studied by several groups using various experimental and theoretical techniques. The reason for this long-lasting interest is that methane is the major constituent of natural gas. Note that natural gas is one of the most promising alternative energy sources and one of its main advantages is that it is much cheaper and environmental friendly than petroleum-based fuels.

Of particular academic and industrial interest in this area of research is the storage of fluid methane in adequate amounts into suitable nanoporous materials. A very important issue here is to find the range of thermodynamic conditions, where the storage of methane in such kind of materials becomes quite satisfactory.

Following the literature, we can notice that methane adsorption in nanoporous materials occurs mainly at supercritical (SC) conditions [1]. It should be emphasized that, due to the low critical temperature of methane (190.56 K), the pure gas cannot be liquefied at room temperature by increasing exclusively alone the pressure. Although numerous investigations concerning the adsorption of methane in nanoporous materials have been published so far (see Refs. [1–4] and references therein), it is important to mention that only a limited number of experimental as well as theoretical studies of the pure SC fluid [5–11] have been reported until the time this work was written. Therefore, a deeper and more quantitative understanding of the physicochemical properties of pure SC methane becomes indispensable to elucidate fundamental aspects of this molecular system.

Moreover, in view of the great scientific and technological potentials of the compressible regime around the critical point of methane, there is still great interest in exploring its properties around this point, as well as its behavior at vapor–liquid phase equilibrium.

Quite recently, Stassen [12] reported a computer simulation study of liquid methane concerning the

* Corresponding author.
E-mail address: isamios@cc.uoa.gr (J. Samios).

0167-7322/$ - see front matter © 2004 Elsevier B.V. All rights reserved.
doi:10.1016/j.molliq.2004.08.014

Table 1
Parameters of the OPLS-AA and MG potential models

	OPLS-AA	MG
ε_{CC} (K)	33.21	51.20
σ_{CC} (nm)	0.35	0.335
q_C (e)	−0.24	–
ε_{HH} (K)	15.10	8.63
σ_{HH} (nm)	0.25	0.2813
q_H (e)	0.06	–
ε_{CH} (K)	22.39	23.80
σ_{CH} (nm)	0.30	0.2995
d_{CH} (nm)	0.109	0.110

accuracy of previously proposed potential models in predicting certain properties of the system. In that study, the author pointed out that the all-atom (AA) five-center semiempirical Lennard–Jones (LJ) potentials, with or without electrostatic interactions, proposed by Jorgensen et al. (OPLS-AA) [13] and Murad–Gubbins (MG) [14], provide the most accurate description of the liquid compared with other site–site potentials with exponential repulsive parts. Moreover, it has been found that the simple one site LJ potential model proposed by Saager and Fischer (SF) [9,15] is quite accurate in predicting the bulk thermodynamic properties of liquid methane. Note that the construction of the SF potential model has been achieved by the adjustment of its parameters in order to predict vapor pressures and liquid densities of the system. We mention that, for the SF model, the calculated pressure and potential energy for SF methane at 150 K and corresponding density of 28 mol l^{-1} are in excellent agreement with experiment (see Table 2 model A in Ref. [12]). For this reason, we decided to select the SF potential model in order to study the two phase (VL) region of pure methane. Note that other reported force fields employed for methane have been already tested in the vapor–liquid equilibrium (VLE) region of the system [16]. We must notice at this point that it is generally desirable to predict accurate T–ρ VL coexistence curves of molecular systems using techniques such as the Gibbs Ensemble Monte Carlo (GEMC) one and in terms of available simple and computationally nondemanding potential models.

In addition, our interest has been extended to explore the behavior of fluid methane at SC conditions. It is well known, however, that to perform systematic theoretical studies of fluids at SC conditions, one has to tackle the problem of the interactions among the molecules at these conditions. Generally speaking, potential models optimized to reproduce liquid state properties are not transferable to the SC state without modifications. Accordingly, it seems appropriate to reassess the reliability of such kind of potential models at SC conditions.

Concretely, the potential models under study in the present work employed for SC methane are the OPLS-AA and MG. Taking into account all the above considerations, we decided to investigate the physicochemical properties of SC methane by performing systematic molecular dynamics (MD) simulations over a wide range of thermodynamic conditions.

The remainder of the paper is organized as follows. The potential models and computational details are described in Section 2 and our results and concluding remarks are presented in Section 3.

2. Computational details and potential models

As mentioned in the Introduction, the fluid was simulated at two totally different regions of the PVT phase space, namely at a wide range of VLE state points and at SC conditions. The VLE state points were investigated using the well established NVT-GEMC technique, which provides a powerful tool for simulating the two coexisting phases. A detailed description of the GEMC computational method is available in the literature [17]. Nevertheless, a brief description of some basic aspects of this technique will be presented herein. According to the NVT-GEMC method, the two phases at equilibrium are simulated at a given temperature and for a fixed number of molecules. During the MC simulation, the whole system is divided into two subsystems, which represent two different homogeneous phases, the liquid (L) phase and the vapor (V) one. At each state point under investigation, the corresponding VLE is achieved by generating a sequence of MC trial moves of

Table 2
Experimental [20] and simulated vapor–liquid equilibrium properties of fluid CH_4 using the Saager Fischer [9,15] potential model from this work

T (K)	ρ_l (sim) (kg m^{-3})	ρ_l (exp) (kg m^{-3})	ρ_{vap} (sim) (kg m^{-3})	ρ_{vap} (exp) (kg m^{-3})	P (sim) (bar)	P (exp) (bar)	ΔH_{vap} (sim) (kJ mol^{-1})	ΔH_{vap} (exp) (kJ mol^{-1})
100	438.9	437.9	0.759	0.720	0.375	0.344	8.521	8.510
110	423.4	423.8	1.277	1.680	0.710	0.881	8.277	8.243
120	408.8	408.8	3.316	3.410	1.970	1.914	7.988	7.935
130	392.4	392.9	5.599	6.218	3.489	3.673	7.641	7.573
140	375.9	375.6	9.962	10.508	6.317	6.412	7.214	7.141
150	357.1	356.5	14.560	16.850	9.604	10.400	6.778	6.619
160	338.0	334.7	23.120	26.151	14.990	15.921	6.200	5.972
170	316.1	308.5	35.070	40.163	22.130	23.283	5.503	5.138
180	292.8	273.3	55.940	63.530	31.480	32.852	4.537	3.961

three different types. The first type of MC moves includes changes in the positions and orientations of arbitrary selected species in order to ensure equilibration in each phase separately. The second type corresponds to the exchange of particles between the two phases aimed to equilibrate the chemical potentials, μ of each subsystem and finally, the last type is related to the volume changes in the coexisting phases to achieve equalization of the pressures in both subsystems. The criteria for accepting or discarding the aforementioned trial MC moves are described in Ref. [18]. It should also be mentioned here that as one approaches the critical point even closer, the simulations become even more complicated due to finite size effects [19].

In the present study, the NVT-GEMC simulations were performed at nine experimental available V–L coexistence state points and for temperatures in the range 100–180 K. Each simulated system was consisted of a total number of 200 methane particles in the two simulation boxes, starting from an arbitrary selected initial configuration where equal number of species (100) was randomly placed in each subsystem. At each simulated state point, the initial density of each subsystem was set equal to the value $(\rho_l+\rho_v)/2$, where ρ_l and ρ_v are the experimental densities of the liquid and the vapor phase, respectively. Each phase was simulated by using standard three-dimensional periodic boundary conditions with images of itself. Each configuration was generated by a randomly selected MC move. The percentage of the occurrence of each of the aforementioned types of MC moves per cycle of MC steps were set to 89%, 10% and 1% for translations, phase and volume change, respectively. As pointed out above, the potential model used in the present study was the one proposed by Saager and Fischer (SF). The SF model is a simple one-site LJ potential with parameters ε/k_B=149.92 K and σ=0.37327 nm. The whole system was equilibrated using 2×10^6 total configurations. After the equilibration period, each production run was extended to 4×10^6 total configurations to obtain the properties of the system.

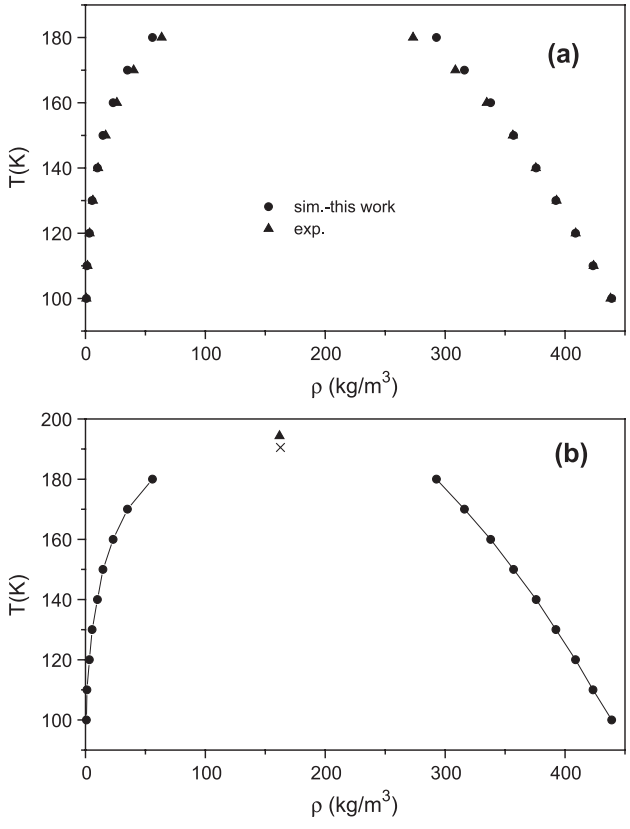

Fig. 1. Vapor–liquid coexistence curves. (a) Experimental data [20] and simulation results from this study. (b) The simulated vapor–liquid coexistence points for methane from this study. Solid lines represent the least-squared fit of the simulated results to the critical scaling relation (Eq. (2)). The predicted and experimental critical points are depicted as symbols, respectively: predicted (up triangle) and experimental (cross).

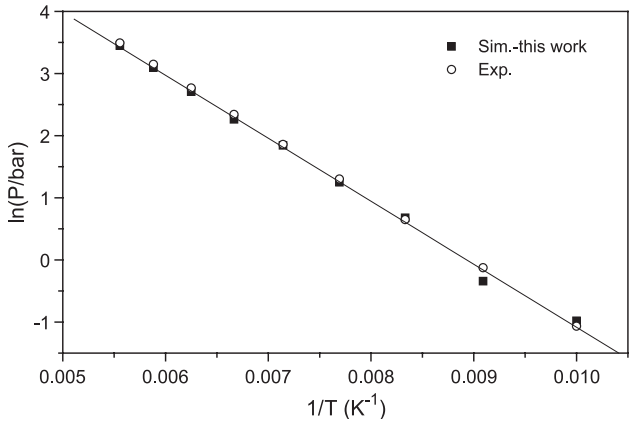

Fig. 2. Clausius–Clapeyron plots of the saturated vapor pressure against the inverse temperature. The solid line corresponds to the fit of the simulated points to the Clausius–Clapeyron equation.

Furthermore, the properties of the fluid were investigated at SC conditions by utilizing NVT- and NPT-MD simulation techniques. Concretely, we performed simulations in a wide range of thermodynamic state points for which experimental data are available [20].

As mentioned in the Introduction, the potentials employed in this study to model the SC fluid were the

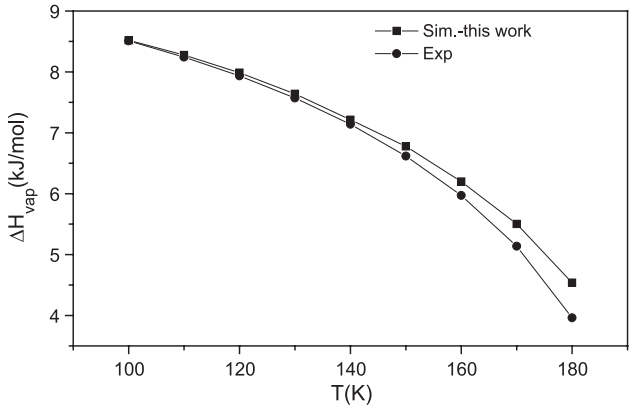

Fig. 3. Heats of vaporization as a function of temperature.

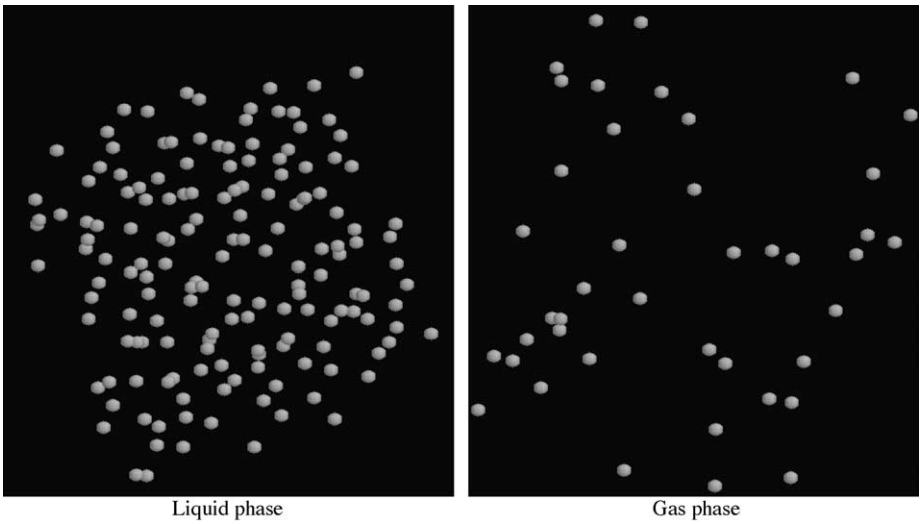

Fig. 4. Snapshot of the two VL coexisting phases from our simulation study at T=180 K.

OPLS-AA and MG. According to the simulations of Stassen [12], these models have been found to be quite reliable in predicting the properties of liquid methane. Thus, these previously reported results led us to select and employ these potentials in our present investigation of SC methane. The OPLS-AA model is a five-site LJ 12-6 potential plus Coulombic terms, whereas the MG one is also a five-site LJ 12-6 but without electrostatic interactions. A complete description of these potential models is given in Table 1.

In an earlier MD simulation study of van Waveren et al. [10], the authors pointed out that the MG model overestimates the pressure of the fluid methane at T=298.15 K. However, the properties of this model have not been widely investigated at SC conditions. Also, Saager and Fischer pointed out in Ref. [9] that their model predicts the experimental pressures of methane at the SC isotherm T=298.15 K with great accuracy ±2% in comparison with experiment. In an earlier treatment, Strauß et al. [5] performed a neutron diffraction study of deuterated fluid methane (CD_4) at 370 K and high pressures and the total weighted intermolecular pair radial distribution function (PRDF), $G(r)$, of the fluid at three state points was obtained. This function may be expressed in terms of the appropriate atom–atom PRDFs.

Therefore, although it has been found that a simple model like the SF one can predict the bulk thermodynamic properties of SC methane accurately, however, the latter model cannot be employed to study the intermolecular structure of the fluid in details. Thus, for this purpose the use of a more detailed site–site potential model is required. All these reasons motivated us to employ the site–site aforementioned two models in our MD study of SC methane.

At each SC condition under investigation, we performed simulations for systems consisting of 256 methane molecules in the central simulation box using periodic boundary conditions. In all cases, a spherical cut-off with half the box length as the cut-off distance was used to truncate the short-range interaction. In the case of the OPLS-AA potential, the well-established Ewald summation method was utilized to account for the long-range electrostatic corrections. Molecular orientations have been formulated by the implementation of the quaternion formalism and the translational and rotational equations of motion were integrated using the leapfrog algorithm. In all cases, the integration time step used was 1 fs. Initial configurations were based on the FCC lattice with densities corresponding to the experimental ones. Each model fluid was simulated for a time interval of 200 ps. From this period, the first 50 ps were regarded as the time interval to reach equilibrium and the rest to calculate the properties of the system.

3. Results and discussion

3.1. Vapor–liquid equilibrium

As mentioned above, the NVT-GEMC simulations of fluid methane were carried out at nine VL coexisting state points for which experimental data are available from the literature. The simulated VLE thermodynamic conditions

Table 3
Critical properties of methane for various force fields (OPLS-UA [16,24,25], TraPPE-UA [16,25], OPLS-AA [13,16,26] TraPPE-EH [16]) reported in previous simulation studies and for the SF [9,15] model used in this work with experimental data [20]

	OPLS-UA, TraPPE-UA	OPLS-AA	TraPPE-EH	SF, this work	Exp.
T_c (K)	191.0	191.0	189.6	194.33	190.60
ρ_c (kg m^{-3})	160.0	170.0	161.0	161.80	162.60
P_c (bar)	45.0	46.0	45.0	46.47	45.99

Table 4
Thermodynamic properties and self-diffusion coefficients of SC methane obtained for the OPLS-AA [13] and MG [14] potential models from the present NVT-MD study in comparison with the experiment

P=11 MPa															
T (K)	295			333			364			403			454		
Model	OPLS-AA	MG	Exp.	OPLS-AA	MG	Exp.	OPLS-AA	MG	Exp.	OPLS-AA	MG	Exp.	OPLS-AA	MG	Exp.
$-U_p$	1.364	1.292		1.077	1.015		0.923	0.872		0.783	0.741		0.651	0.619	
P	11.4	12.3	11	11.4	12.1	11	11.3	11.8	11	11.2	11.7	11	11.2	11.5	11
E	5.980	6.052		7.213	7.274		8.139	8.189		9.250	9.291		10.652	10.683	
D	16.58	16.66	15.8	22.25	21.70	20.5	27.43	25.82	25.2	33.37	31.17	31.5	41.90	39.26	34.5
ρ	0.086228	0.086228	0.086228	0.07043	0.07043	0.07043	0.061973	0.061973	0.061973	0.054251	0.054251	0.054251	0.04698	0.04698	0.04698
P=31 MPa															
T (K)	295			333			364			403			454		
Model	OPLS-AA	MG	Exp.	OPLS-AA	MG	Exp.	OPLS-AA	MG	Exp.	OPLS-AA	MG	Exp.	OPLS-AA	MG	Exp.
$-U_p$	3.391	3.277		2.781	2.685		2.406	2.319		2.059	1.969		1.728	1.650	
P	32.3	42.8	31	32.4	39.2	31	32.3	37.3	31	32.5	36.4	31	32.3	35.3	31
E	3.952	4.067		5.509	5.605		6.656	6.743		7.974	8.063		9.574	9.652	
D	5.44	4.85	5.74	7.87	6.84	7.77	9.33	8.47	9.23	11.92	9.98	11.8	14.86	13.81	14.6
ρ	0.22016	0.22016	0.22016	0.18552	0.18552	0.18552	0.16406	0.16406	0.16406	0.14351	0.14351	0.14351	0.12389	0.12389	0.12389
P=107 MPa															
T (K)	295			327			364			394			427		
Model	OPLS-AA	MG	Exp.	OPLS-AA	MG	Exp.	OPLS-AA	MG	Exp.	OPLS-AA	MG	Exp.	OPLS-AA	MG	Exp.
$-U_p$	5.461	5.257		5.056	4.868		4.643	4.459		4.345	4.165		4.051	3.870	
P	103.4	162.0	107	106.6	156.4	107	108.9	151.2	107	110.3	147.9	107	111.3	144.8	107
E	1.882	2.086		3.084	3.272		4.418	4.602		5.463	5.643		6.578	6.759	
D	2.34	1.96	2.61	2.97	2.53	3.22	3.67	3.15	3.92	4.21	3.45	4.53	5.00	4.37	5.2
ρ	0.35052	0.35052	0.35052	0.33195	0.33195	0.33195	0.31216	0.31216	0.31216	0.29742	0.29742	0.29742	0.2825	0.2825	0.2825

The properties shown are the average potential energy, U_{pot} (kJ mol^{-1}); the pressure, P (MPa); the total energy, E (kJ mol^{-1}); the density, ρ (g cm^{-3}) and the self-diffusion coefficient D (10^{-8} m^2 s^{-1}) for the isobars 11, 31 and 107 MPa and five corresponding temperatures at each isobar.

Table 5
Thermodynamic properties and self-diffusion coefficients of SC methane obtained from NPT-MD simulations using the OPLS-AA [13] and MG [14] potential models from the present study, in comparison with the experiment

T (K)	195			277			400		
Model	OPLS-AA	MG	Exp.	OPLS-AA	MG	Exp.	OPLS-AA	MG	Exp.
$-U_p$	6.071	4.905		3.701	3.050		2.019	1.780	
P	31	31	31	31	31	31	31	31	31
E	−1.207	−0.055		3.199	3.845		7.935	8.255	
D	1.61	2.22		4.72	5.46		11.70	12.56	
ρ	0.36280	0.30174	0.34585	0.23709	0.20261	0.24009	0.13999	0.12950	0.14489

The properties shown are the average potential energy, U_{pot} (kJ mol^{-1}); the pressure, P (MPa); the total energy, E (kJ mol^{-1}); the density, ρ (g cm^{-3}) and the self-diffusion coefficient D (10^{-8} m^2 s^{-1}) for the isobar P=31 MPa and three corresponding temperatures.

together with the results obtained are summarized in Table 2. The performance of the SF potential model used in the present work with respect to the prediction of the experimental VL coexistence densities (ρ_l, ρ_v), vapor pressure (P_{vap}) and heats of vaporization (ΔH_{vap}), calculated as in Ref. [18], are shown in Table 2 and Figs. 1–3. Also, we present in Fig. 4 a snapshot of the two VL coexisting phases from our simulation study at T=180 K. Concretely, Fig. 1a shows the experimental (squares) and simulated (circles) VL coexistence densities of methane at the temperature range 100–180 K. Note that in the case of the simulated liquid densities the statistical uncertainties are approximately of a similar extent compared with the symbol sizes. In the case of the gas-saturated densities, pressures and heats of vaporization, we estimated the standard deviations of these properties to be about 2–9%. As a result, the SF potential model for fluid methane yields good agreement with experimental data [20] with respect to the prediction of the saturated liquid and vapor densities and pressures of the system over the temperature range of interest. Also, the SF model predicts satisfactory the heats of vaporization at lower temperatures but overestimates this property by about 0.5 kJ mol^{-1} at higher temperatures.

We complete this study by the estimation of the critical properties of the fluid (T_c, ρ_c, P_c) from least-squared fits of the subcritical simulation results to the well-known critical scaling relation [21] for the critical temperature T_c

$$\rho_l - \rho_v = B(T_c - T)^{\beta}, \quad (1)$$

to the equation of the rectilinear diameters [22] for the critical density ρ_c

$$\frac{\rho_l + \rho_v}{2} = \rho_c + A(T - T_c), \quad (2)$$

and the Clausius–Clapeyron equation [23] for the critical pressure, P_c.

$$\ln P = C + \frac{D}{T} \quad (3)$$

The estimated critical parameters (T_c=194.33 K, ρ_c=161.795 kg m^{-3}, P_c=46.47 bar) for the SF model of methane from this work are presented in Table 3 and Fig. 1b together with results from previous simulation studies using several available models [16] and in comparison with experiment. It should be mentioned here that the critical exponent, β, appearing in Eq. (1) has been estimated to be 0.3268. As can be observed, the calculated critical temperatures, T_c, for the OPLS-UA, TRAPPE-UA, OPLS-AA and TRAPPE-EH models are in quite good agreement with the experiment. A similar pattern can be observed from the above comparison of T_c for the SF model, although in this

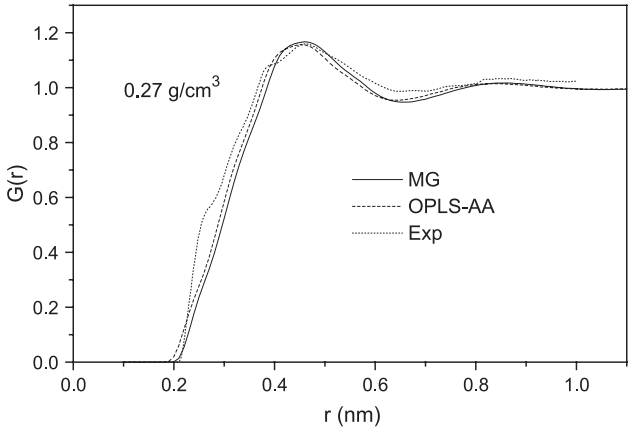

Fig. 5. Total PRDFs at T=370 K and 0.27 g cm^{-3} obtained by the OPLS-AA and MG models in comparison with the experiment.

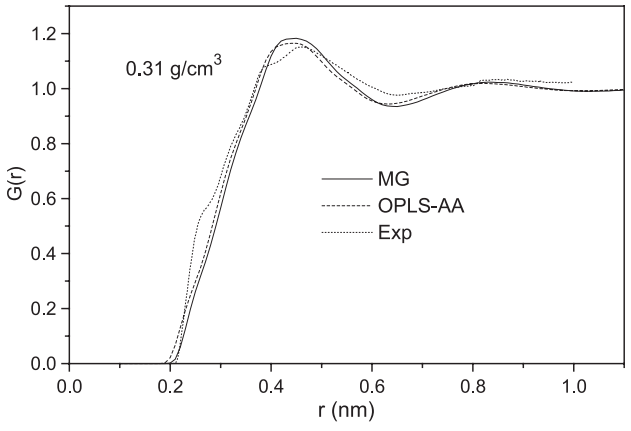

Fig. 6. Total PRDFs at T=370 K and 0.31 g cm^{-3} obtained by the OPLS-AA and MG models in comparison with the experiment.

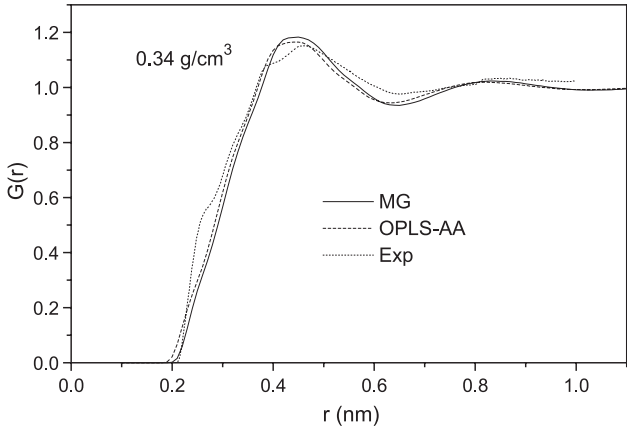

Fig. 7. Total PRDFs at T=370 K and 0.34 g cm^{-3} obtained by the OPLS-AA and MG models in comparison with the experiment.

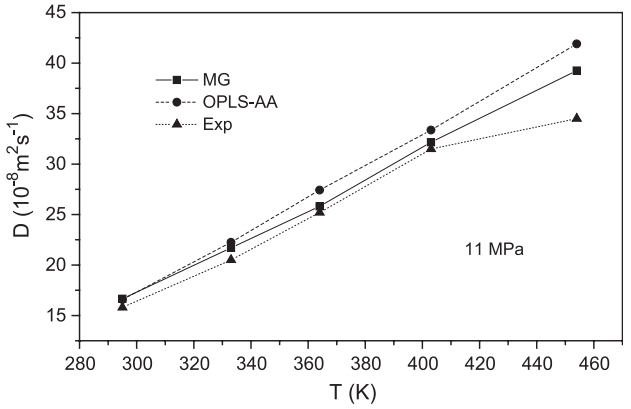

Fig. 9. Self-diffusion coefficient of methane as a function of temperature along the SC isobar of 11 MPa. Depicted are the results obtained by the OPLS-AA and MG models in comparison with the experiment.

case the predicted value is slightly overestimated in comparison with the experimental one. Concerning the critical densities and pressures obtained, we may conclude that the SF model is somewhat superior to the other aforementioned models.

3.2. Supercritical methane

3.2.1. Thermodynamic properties

As mentioned above, we have carried out a series of NVT-MD simulations of SC methane in a wide range of temperatures and pressures. The most important thermodynamic functions, such as the average total energy, potential energy U^{sim} and pressure P^{sim}, have been evaluated and they are presented in Table 4 in comparison with available experimental data.

More specifically, the NVT-MD simulations have been performed at several state points along three SC isobars using available experimental densities corresponding to the pressures 11, 31 and 107 MPa. By inspecting the results obtained from the two potential models, we may clearly conclude that the OPLS-AA potential is much more accurate in predicting the pressure of the system than the MG one in comparison with the experimental data. Furthermore, the OPLS-AA and MG models are more accurate in predicting the pressure along the isobar of 11 MPa. However, as the pressure increases we observe larger deviations between simulated and experimental pressure, especially for the MG model.

In order to investigate more systematically the efficiency of these models in predicting the thermodynamic properties of SC methane, we have carried out supplementary NPT-MD simulations for three different temperatures along the SC isobar P=31 MPa to obtain the density of the fluid. The results obtained are summarized in Table 5 in comparison with the experiment. According to these results, the OPLS-AA model provides a more accurate result for the density of SC methane than the MG model at these SC conditions.

Concretely, by inspecting the results obtained from our simulation studies we may conclude that the OPLS-AA model has been found to be somewhat superior to the MG one in predicting certain thermodynamic properties of SC methane at the state conditions under investigation.

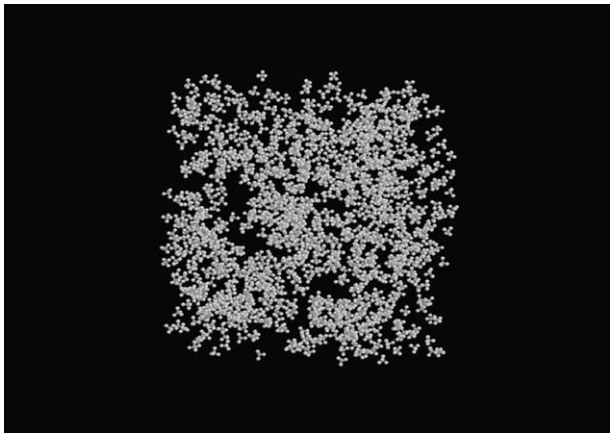

Fig. 8. Snapshot of a configuration of SC methane at 195 K and 0.11494 g cm^{-3} obtained from this study.

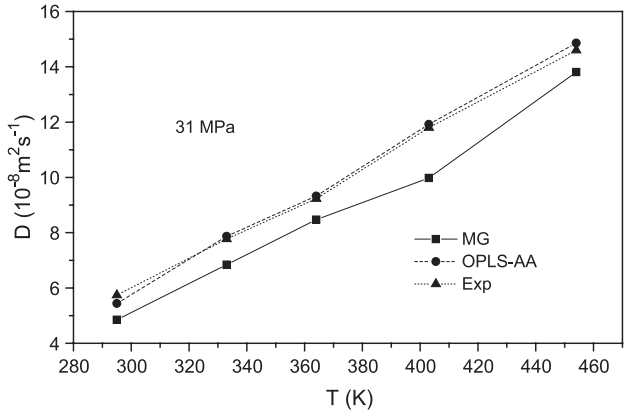

Fig. 10. Self-diffusion coefficient of methane as a function of temperature along the SC isobar of 31 MPa. Depicted are the results obtained by the OPLS-AA and MG models in comparison with the experiment.

3.2.2. Intermolecular structure

In the framework of the present study, the intermolecular structure of SC methane was investigated in terms of the calculated site–site pair radial distribution functions (PRDFs). From the experimental point of view, Strauß et al. [5] reported a neutron diffraction study of CD_4 at T=370 K and several densities of the system. In that study, the authors reported the total PRDFs, $G(r)$, at the aforementioned state points. They have also expressed these functions on the basis of the weighted three site–site PRDFs (C–C, C–H and H–H) according to the relation:

$$G(r) = 0.040 g_{CC}(r) + 0.319 g_{CH}(r) + 0.641 g_{HH}(r) \qquad (4)$$

We have calculated all these structural functions at each SC thermodynamic condition under investigation but only the results related to the above experimental study are presented and discussed herein. Thus, the results obtained for the OPLS-AA and MG potential models in comparison with the experimental data are depicted in Figs. 5–7.

By investigating the behavior of these functions at T=370 K and densities of 0.27, 0.31 and 0.34 g cm^{-3}, we may conclude that both the OPLS-AA and MG models predict the location of the first peak of the total PRDFs at 0.46, 0.45 and 0.44 nm at each density, respectively. These values are in good agreement with the experimental ones at about 0.46 nm (see Fig. 5 in Ref. [5]). In the case of the lower density, both models predict quite satisfactory the amplitude of the first peak in comparison with experiment. At 0.31 and 0.34 g cm^{-3}, both models provide slightly overestimated first peak intensities compared with experiment. In contrast, we may observe that in all cases both models underestimate the amplitude of the first minimum of these functions in comparison with experiment. Furthermore, we mention that the characteristic small shoulder observed at very short distances of 0.28 nm on the experimental total PRDFs has not been clearly predicted from the simulations using the OPLS-AA and MG potential models. Therefore, this behavior still remains an open problem in the study of the intermolecular structure of this fluid. Concerning the existence of local density inhomogeneities and related problems in the near-critical region of SC methane, we have performed an NVT-MD simulation study of 1000 methane particles at 195 K and density 0.11494 g cm^{-3} by employing the OPLS-AA model. The results obtained from this treatment will be presented in a forthcoming publication. Here, we present in Fig. 8 a snapshot of a representative configuration of the simulated system, where the formation of characteristic density inhomogeneities is clearly seen.

In general, we may conclude that the accuracy of both potential models tested in our study in predicting the intermolecular structure of SC methane is quite similar, and the agreement of the results predicted with the experiment is to some extent satisfactory. However, to investigate the intermolecular structure of the fluid in a more systematic way, we need more experimental data to compare with the results obtained from our molecular simulation studies.

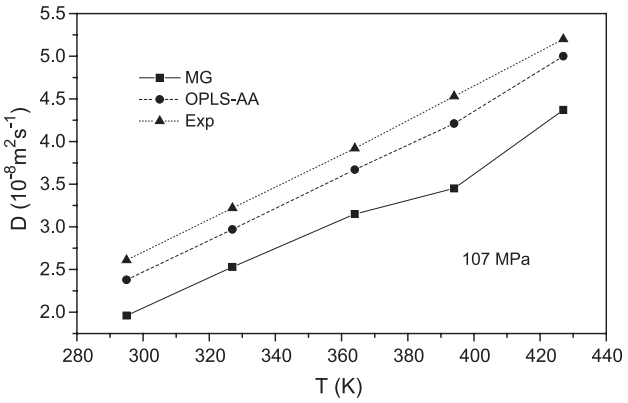

Fig. 11. Self-diffusion coefficient of methane as a function of temperature along the SC isobar of 107 MPa. Depicted are the results obtained by the OPLS-AA and MG models in comparison with the experiment.

3.2.3. Transport properties

In the framework of the present investigation, we have estimated the self-diffusion coefficients, D, of SC methane for several state points along the SC isobars 11, 31 and 107 MPa. These coefficients were calculated on the basis of the mean square displacements of the particles and were compared with available experimental data obtained from NMR spin echo measurements [6]. The results obtained are summarized in Table 4 and depicted in Figs. 9–11. By inspecting carefully these results, we can see that at the isobar P=11 MPa the efficiency of the two models employed in our treatment in predicting the self-diffusion coefficients is similar, and quite good in comparison with the experiment. However, at higher pressures the deviation between experimental and simulated values becomes larger for the MG model. Concretely, we may conclude that the OPLS-AA model is somewhat superior to the MG one in predicting this particular transport property in the investigated range of thermodynamic conditions.

Acknowledgements

This work was carried out within the Project No. 70/4/6485 AU. The CPU time allocation on the computer systems of the University of Athens, Greece, and on the Cray T3E-1200 at the Research Center ZAM Jülich, Germany, is also gratefully acknowledged.

References

[1] D. Lozano-Castello, J. Alcaniz-Monge, M.A. de la Casa-Lillo, D. Cazorla-Amoros, A. Linares-Solano, Fuel 81 (2002) 1777.
[2] P.K. Ghorai, M. Sluiter, S. Yasonath, Y. Kawazoe, J. Am. Chem. Soc. 125 (2003) 16192.

[3] D.P. Cao, X.R. Zhang, J.F. Chen, W.C. Wang, J. Yun, J. Phys. Chem. B107 (2003) 13286.
[4] M. Jorge, N.A. Seaton, Mol. Phys. 100 (2002) 3803.
[5] G. Strauß, A. Bassen, H. Zweier, H. Bertagnolli, K. Tödheide, A.K. Soper, J. Turner, Phys. Rev. E53 (1996) 3505.
[6] A. Greiner-Schmid, S. Wappmann, M. Has, H.D. Lüdemann, J. Chem. Phys. 94 (1991) 5643.
[7] A.D. Simmons, P.T. Cummings, Chem. Phys. Lett. 129 (1986) 92.
[8] T. Hauschild, J.M. Prausnitz, Mol. Simul. 11 (1993) 177.
[9] B. Saager, J. Fischer, Fluid Phase Equilib. 57 (1990) 35.
[10] G.M. van Waveren, J.P.J. Michels, N.J. Trappeniers, Physica B139/140 (1986) 144.
[11] A. Allal, C. Boned, A. Baylaucq, Phys. Rev. E64 (2001) 11203.
[12] H. Stassen, J. Mol. Struct. 464 (1999) 107 (Theochem).
[13] W.L. Jorgensen, D.S. Maxwell, J. Tirado-Rives, J. Am. Chem. Soc. 118 (1996) 11225.
[14] S. Murad, K.E. Gubbins, ACS Symp. Ser. 86 (1978) 62.
[15] J. Fischer, R. Lustig, H. Breitenfelder-Manske, W. Lemming, Mol. Phys. 52 (1984) 485.
[16] B. Chen, J.I. Siepmann, J. Phys. Chem. B103 (1999) 5370.
[17] A.Z. Panagiotopoulos, http://kea.princeton.edu/jerring/gibbs/index.html.
[18] J. Volholz, V.I. Harismiadis, B. Rumpf, A.Z. Panagiotopoulos, G. Maurer, Fluid Phase Equilib. 170 (2000) 203.
[19] B. Smit, Ph. De Smedt, D. Frenkel, Mol. Phys. 68 (1989) 931.
[20] E.W. Lemmon, M.O. McLinden, D.G. Friend, Thermophysical properties of fluid systems in NIST Chemistry WebBook, NIST Standard Reference Database Number 69, Eds. P.J. Linstrom amd W.G. Mallard, March 2003, National Institute of Standards and Technology, Gaithersburg MD, 20899 (http://webbook.nist.gov).
[21] J.S. Rowlinson, B. Widom, Molecular Theory of Capillarity, Oxford Univiversity Press, New Work, 1989.
[22] J.S. Rowlinson, F.L. Swinton, Liquids and Liquid Mixtures, 3rd ed., Butterworth, London, 1982.
[23] P.W. Atkins, Physical Chemistry, 4th ed., Freeman, New York, 1990.
[24] W.L. Jorgensen, J.D. Madura, C.J. Swenson, J. Am. Chem. Soc. 106 (1984) 813.
[25] M.G. Martin, J.I. Siepmann, J. Phys. Chem. B102 (1998) 2569.
[26] B. Chen, M.G. Martin, J.I. Siepmann, J. Phys. Chem. B102 (1998) 2578.